Compliance Synthesis of a Class of Planar Compliant Parallelogram Mechanisms Using the Position Space Concept*

Guangbo Hao, Jingjun Yu, Yufei Liu

Abstract— **Compliant mechanisms can be reconfigured with variation of compliance performance, by changing the positions of each compliant module thereof within its position space. This paper synthesizes the compliance of two types of parallelogram mechanisms by changing the positions of compliant joints within their position spaces. Through analytical modelling, detailed analysis is implemented to uncover the influence of positions on compliance characteristics. Finally, some desired designs are presented.**

I. Introduction

Compliant mechanisms uses their flexible members to transfer motion, load, and/or energy, which have gained increasing attentions in academia and industry [1-5]. Different from rigid-body mechanisms, the structure of a compliant mechanism can be reconfigurable through changing the positions of each (decomposed) compliant module thereof within its pre-determined position space [6-9], where the position space theory can be introduced through a discussion and mathematical derivation of relevant screw theory kinematics [8,9]. Each module can be an independent one or coupled with another when determining the position space [9]. The position-space-based approach reconfigures a compliant mechanism into sub-mechanisms that ultimately produce the same overall DOF (degrees of freedom, i.e. mobility). The position space method also considers the positions of each compliant joint/module relative to its adjacent compliant joint/module. The presentation of position spaces can offer an efficient and systematic method to arrange the relative positions between any two compliant joints/modules so that one can easily generate practical and useful configurations [6,7]. Benefits of reconfiguring a mechanism into a new shape/structure may include improvement of performances in parasitic motion, reduced lost motion, stress distribution, manufacturability, and compactness (or symmetry) [6-10]. Position spaces include translational and rotational cases, or single-DOF and multi-DOF cases as reported in [6-10].

Synthesis can form a starting point for further nonlinear analysis and optimization. Figure 1(a) shows the hierarchy relation among type synthesis, position space based synthesis, and dimensional synthesis in designing compliant mechanisms. The position space based synthesis can provide an extra option of optimizing or synthesizing compliant mechanisms. In order to explain the position space concept better, Fig. 2(a) presents a generic 2-DOF (degree of freedom) serial compliant translational mechanism, composed of two parallelogram modules, modules 1 and 2. Let the output motion stage keep fixed, without changing the mobility of the system, module 1 can rotate about the fixed Y-axis while module 2 can rotate about the mobile X-axis (always parallel to the fixed X-axis), that is connected to module I. The position space of each translational module is illustrated as a circle, whose specific position is defined by a rotational angle variable. When the rotational angle of each module are given, the specific configuration of the system is obtained (four specific configurations shown in Fig. 1(c)). The designs in [11,12] actually use the specific configuration in the position space of two serial modules for high-payload applications.

Inspired by the above idea, Refs. [13-15] have synthesized translational joints and tip-tilt-piston mechanisms by defining a set of parameters under a framework of the position space. With the similar motivation, this paper aims to implement compliance synthesis of a class of planar compliant parallelogram mechanisms, including the parallelogram mechanism using identical short-beam hinges and the one using identical cross-axis joints. The results of synthesis in this paper intend to confirm the optimal configuration as well as to reveal the influences of positions of hinges/joints upon compliance performance characteristics.

This paper is organized as below. Sec. 2 proposes the design of a generic parallelogram mechanism using short-beam hinges. Its compliance modelling and analysis are detailed in Sec. 3. Sec. 4 models and analyzes an improved parallelogram mechanism using cross-axis joints. Finally, conclusions are drawn in Sec. 5 with the presentation of some desired designs.

*This research is supported by Visiting Scholar Foundation of Key Laboratory of Optoelectronic Technology and Systems (Chongqing University), Ministry of Education of China, which is much appreciated. This work was also partially supported by the China National Key Research and Development Program of China (Grant No. 2016YFE0125200 and 2016YFC0101100), and the China Fundamental Research Funds for the Central Universities (Grant No. 106112015CDJXY120007).

Guangbo Hao is with Key Laboratory of Optoelectronic Technology & Systems (Chongqing University), Ministry of Education, Chongqing, 400044, China, and with School of Engineering, University College Cork, Cork, Ireland

Jingjun Yu is with Robotics Institute, Beihang University, Beijing, 100083 China

Yufei Liu is with Center for Intelligent Sensing Technology, College of Optoelectronic Engineering, Chongqing University, Chongqing, 400044, China

Corresponding authors: Guangbo Hao (G.Hao@ucc.ie); Yufei Liu (yufei.liu@cqu.edu.cn)

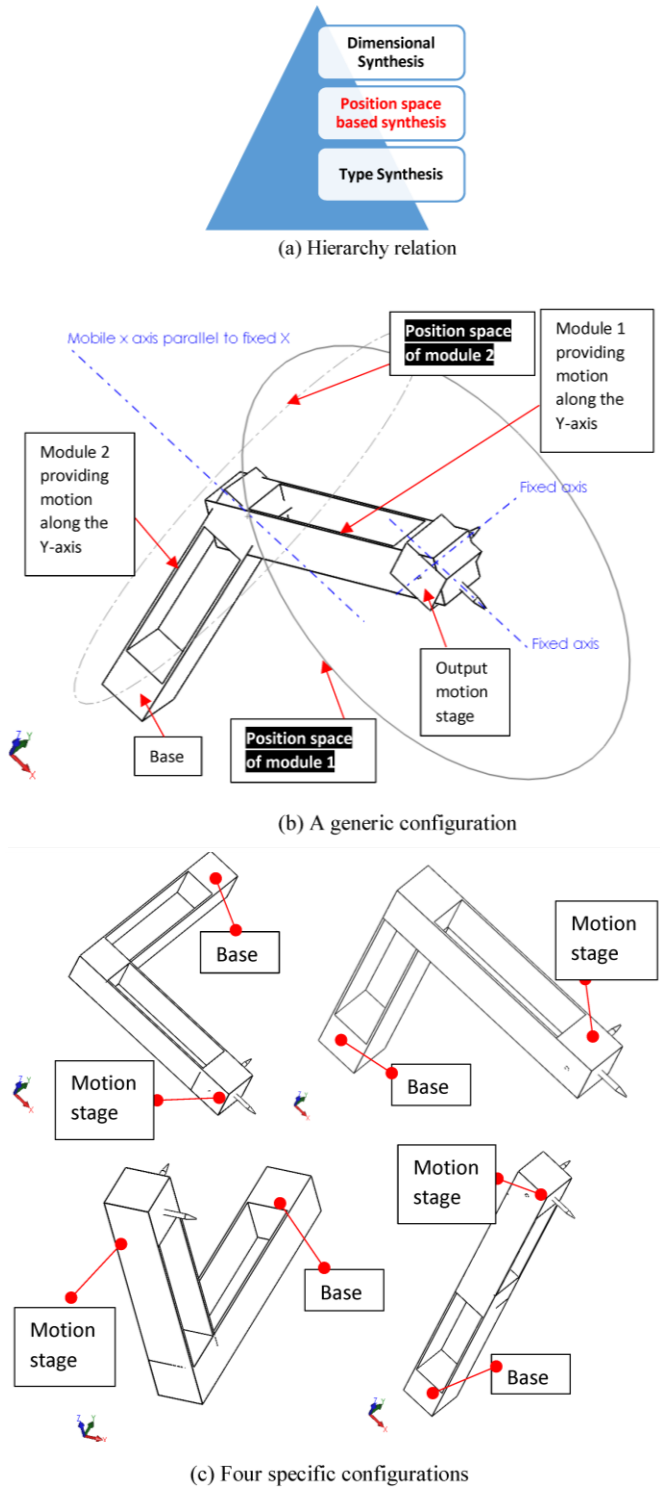

Figure 1. Illustration of position space using a two-DOF serial translational mechanism

II. Design of a Parallelogram Mechanism with the Generic Arrangement of Hinges

In this section, a parallelogram mechanism with the generic arrangement of four short-beam hinges is presented as shown in Fig. 2. Each short-beam hinge can be regarded a revolute joint about its center, the position space of which can be illustrated as a circle with its center located at the beam center [8, 9], as shown in Fig. 2(a).

In the parallelogram, the crank link's length is determined by H and the coupler link's length is denoted by W. Each crank is the leg and the coupler is the motion stage. The horizontal translation of the motion stage is the desired primary motion with others as the undesired parasitic motions. All hinges are identical with its length of L, its in-plane thickness of T, and its out-of-plane thickness of U. A global coordinate system O-XYZ is defined at the center of the parallelogram mechanism. Two leg coordinate systems (O_1-$X_1Y_1Z_1$ and O_2-$X_2Y_2Z_2$) are defined as shown in Fig. 2. Two local coordinate systems for two hinges in Leg 1 are also defined at own stiffness centers, also centers of the short beams (Fig. 2(c)).

Two legs are symmetrical with respect to the X-axis. Here, the distance of centers of two hinges in vertical direction (X-axis) is H ($H \geq L$ for the same plane arrangement of beams), and that in the horizontal direction (Y-axis) is W. In each leg, the position of each hinge can be rotated about its center based on the position space concept as illustrated in Fig. 2(a). As shown in Fig. 2(b), two rotational variables/angles (α and β) are used to define any positions of two hinges in leg 1, and two rotational variables ($-\alpha$ and $-\beta$) are used to define the positions of two hinges in leg 2.

III. Compliance Modelling of the Generic Parallelogram Mechanism

This section models the compliance matrix of the generic parallelogram mechanism based on the linear modelling method. Each hinge's compliance matrix, with respect to its local coordinate system as shown in Fig. 2(c), is written below [16]

$$C = \begin{bmatrix} L^3/(d \cdot EI) & 0 & 0 \\ 0 & L^3/(a \cdot EI) & 0 \\ 0 & 0 & L/EI \end{bmatrix} \quad (1)$$

where a=12 and d=12/$(T/L)^2$. E is the Young's modulus of material, under the assumption of planar stress. I=UT^3/12, which is the second moment inertia of area of the uniform cross section of the hinge.

Using Equation (1), we can derive the compliance matrix of each hinge in Leg 1 under a new coordinate system (at the same hinge center) with axes parallel to these in the global coordinate system O-XYZ:

$$\begin{aligned} C_{11} &= R_{11} C (R_{11})^{\mathrm{T}} \\ C_{12} &= R_{12} C (R_{12})^{\mathrm{T}} \end{aligned} \quad (2)$$

where $R_{11} = \begin{bmatrix} \cos\alpha & -\sin\alpha & 0 \\ \sin\alpha & \cos\alpha & 0 \\ 0 & 0 & 1 \end{bmatrix}$, $R_{12} = \begin{bmatrix} \cos\beta & -\sin\beta & 0 \\ \sin\beta & \cos\beta & 0 \\ 0 & 0 & 1 \end{bmatrix}$,

which are both the rotational transformation matrices to covert the compliance matrix of each hinge from its local coordinate system to the new coordinate system. The two rotational matrices determine the specific rotational position of each hinge in its position space.

We can further obtain the compliance matrix of each hinge with regard to Leg 1's coordinate system O_1-$X_1Y_1Z_1$ as below, using the results in Eq. (2):

$$C_{O11} = \left((D_{11})^{\mathrm{T}} C_{11}^{-1} (D_{11}) \right)^{-1}$$
$$C_{O12} = \left((D_{12})^{\mathrm{T}} C_{12}^{-1} (D_{12}) \right)^{-1} \quad (3)$$

where

$$D_{11} = \begin{bmatrix} 1 & 0 & 0 \\ 0 & 1 & -H/2 \\ 0 & 0 & 1 \end{bmatrix}, D_{12} = \begin{bmatrix} 1 & 0 & 0 \\ 0 & 1 & H/2 \\ 0 & 0 & 1 \end{bmatrix},$$

which are the two locational transformation matrices between the hinge center and the leg center.

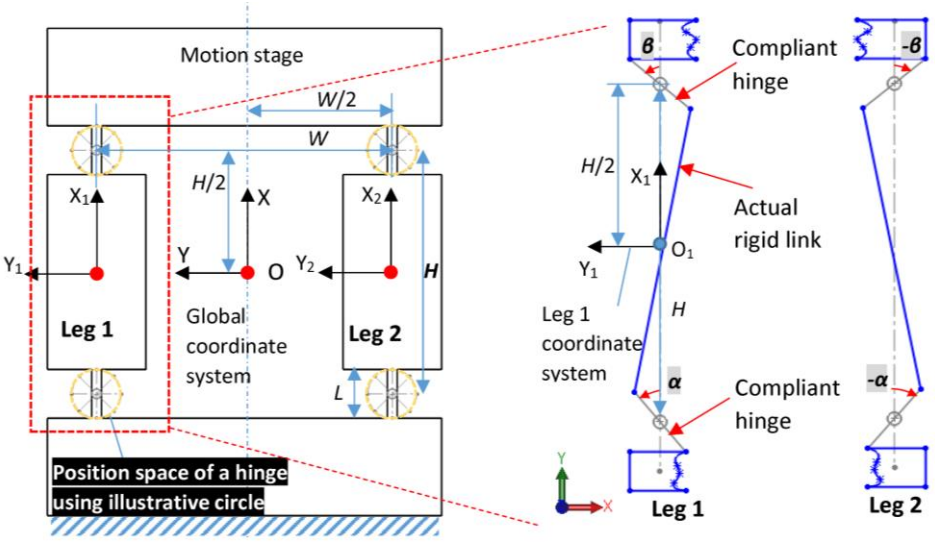

(a) Parallelogram mechanism with straight hinges

(b) Schematic diagram with generic arrangement of hinges

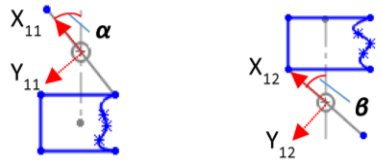

(c) Local coordinate systems for two hinges in Leg 1: bottom hinge on the left, top hinge on the right

Figure 2. A parallelogram mechanism with lumped compliance

Based on the compliance rule of serial systems, Leg 1' compliance matrix with respect to its own coordinate system (O_1-$X_1Y_1Z_1$) is obtained:

$$C_{\mathrm{Leg1}} = C_{O11} + C_{O12} \quad (4)$$

Leg 2' compliance modelling is similar to Leg 1's as shown above. Similar to the process of obtaining Eq. (2), we have the following compliance matrices for two hinges in Leg 2 considering the generic rotational positions:

$$C_{21} = R_{21} C (R_{21})^{\mathrm{T}}$$
$$C_{22} = R_{22} C (R_{22})^{\mathrm{T}} \quad (5)$$

where

$$R_{21} = \begin{bmatrix} \cos(-\alpha) & -\sin(-\alpha) & 0 \\ \sin(-\alpha) & \cos(-\alpha) & 0 \\ 0 & 0 & 1 \end{bmatrix}, R_{22} = \begin{bmatrix} \cos(-\beta) & -\sin(-\beta) & 0 \\ \sin(-\beta) & \cos(-\beta) & 0 \\ 0 & 0 & 1 \end{bmatrix}.$$

With respect to Leg 2's coordinate system O_2-$X_2Y_2Z_2$, Eq. (5) can be transformed as

$$C_{O21} = \left(\left(D_{21} \right)^{\mathrm{T}} C_{21}{}^{-1} \left(D_{21} \right) \right)^{-1}$$
$$C_{O22} = \left(\left(D_{22} \right)^{\mathrm{T}} C_{22}{}^{-1} \left(D_{22} \right) \right)^{-1} \quad (6)$$

where

$$D_{21} = \begin{bmatrix} 1 & 0 & 0 \\ 0 & 1 & -H/2 \\ 0 & 0 & 1 \end{bmatrix}, D_{22} = \begin{bmatrix} 1 & 0 & 0 \\ 0 & 1 & H/2 \\ 0 & 0 & 1 \end{bmatrix}.$$

Then, Leg 2's compliance matrix with respect to its own coordinate system (O_2-$X_2Y_2Z_2$) is obtained as:

$$C_{\mathrm{Leg2}} = C_{O21} + C_{O22} \quad (7)$$

On the basis of Eqs. (4) and (7), the stiffness matrix of each leg are obtained:

$$K_{\mathrm{Leg1}} = (C_{\mathrm{Leg1}})^{-1}$$
$$K_{\mathrm{Leg2}} = (C_{\mathrm{Leg2}})^{-1} \quad (8)$$

Finally, the stiffness matrix of the parallelogram mechanism (with regard to the global coordinate system O-XYZ) is derived in terms of the stiffness rule of parallel systems

$$K_{\mathrm{s}} = \left(T_1 \right)^{\mathrm{T}} K_{\mathrm{Leg1}} T_1 + \left(T_2 \right)^{\mathrm{T}} K_{\mathrm{Leg2}} T_2 \quad (9)$$

where

$$T_1 = \begin{bmatrix} 1 & 0 & -W/2 \\ 0 & 1 & 0 \\ 0 & 0 & 1 \end{bmatrix}, T_2 = \begin{bmatrix} 1 & 0 & W/2 \\ 0 & 1 & 0 \\ 0 & 0 & 1 \end{bmatrix}.$$

The inversion of Eq. (9) yields the following symmetrical matrix:

$$C_{\mathrm{s}} = K_{\mathrm{s}}^{-1} = \begin{bmatrix} C_{\mathrm{s11}} & 0 & 0 \\ 0 & C_{\mathrm{s22}} & C_{\mathrm{s23}} \\ 0 & C_{\mathrm{s32}} & C_{\mathrm{s33}} \end{bmatrix} \quad (10)$$

where the entry in the first row corresponds to the undesired translation along the X-axis, and the entries in the second row correspond to the desired translation along the Y-axis, the entries in the third row correspond to the undesired rotation about the Z-axis.

Using the normalization method [17], the dimensionless/normalized compliance entries are represented below, so that they can be compared each other:

$$c_{11} = \frac{C_{\mathrm{s11}}}{\left(H^3 / EI \right)}; c_{22} = \frac{C_{\mathrm{s22}}}{\left(H^3 / EI \right)}; c_{23} = \frac{C_{\mathrm{s23}}}{\left(H^2 / EI \right)}; c_{33} = \frac{C_{\mathrm{s33}}}{\left(H / EI \right)} \quad (11)$$

where H is the characteristic length for normalization.

In the following, three cases are discussed for the modelling results using the following parameters: L = 5 mm; T = 1 mm; H = 35 mm; W = 20 mm; U = 10 mm; E = 69 GPa.

It is noted that if β=α=0 and H=L, the generic parallelogram mechanism reduces to the classic leaf-type parallelogram mechanism with distributed compliance.

(1) Case I: β=−α

Under case I, a simple diagonal compliance matrix can be symbolically derived as below, which shows no parasitic motion accompanying the primary motion:

$$C_{\mathrm{s}} = \begin{bmatrix} \frac{L\left(\sin(\alpha)^2 L^2 + \cos(\alpha)^2 T^2\right)}{12EI} & 0 & 0 \\ 0 & \frac{L\left(\cos(\alpha)^2 L^2 + \sin(\alpha)^2 T^2 + 3H^2\right)}{12EI} & 0 \\ 0 & 0 & \frac{1}{\frac{3W^2 EI}{L\left(\sin(\alpha)^2 L^2 + \cos(\alpha)^2 T^2\right)} + \frac{EI}{L}} \end{bmatrix} \quad (12a)$$

In Eq. (12a), there are 7 geometrical parameters, L, H, W, T, U, α and β, which affect the compliance entries. Equation (12a) shows that the parameter H only affects C_{s22}, and the parameter W only influences C_{s33}.

In this paper, we focus on studying on influence of the position parameters (α and β) of two hinges. Figure 3 shows the ratios of dimensionless compliance entries (desired one divided by undesired one). c_{22}/c_{11} periodically changes with α ϵ[0, 2π) as described in Fig. 3(a), where the maximal (optimal) value occurs at α=0 or π and the minimal one occurs at α=π/2, or 3π/2. The maximal ratio in Fig. 3(a) is as large as 3750, and the minimal one is lower than 200. Similarly, c_{22}/c_{33} also periodically varies with α as shown in Fig. 3(b). The maximal c_{22}/c_{33} value is larger than 300 occurring at α=0 or π; and the minimal one is lower than 20 occurring at α=π/2, or 3π/2. It is revealed that in the domain close to α=π/2 or 3π/2, the compliance ratio is nearly constant.

The above analysis results confirm that the conventional/normal configuration (with α=β=0) is the optimal one. Although in this section the objective is to design a 1-DOF compliant translational joint, the modelling result can be used to guide the design of a multi-DOF compliant joint through optimize all geometrical parameters.

(2) Case II: β=α

Under case II, a diagonal compliance matrix cannot be obtained and its symbolic expression (as shown in Eq. (A.1)) can not reduce to the form as neat as Eq. (12a). Figures 4(a) and 4(b) show the similar findings of compliance ratios as shown in Fig. 3. However, the parasitic motion entry c_{23} appears as shown in Fig. 4(c), in the order of 10^{-4} (rad).

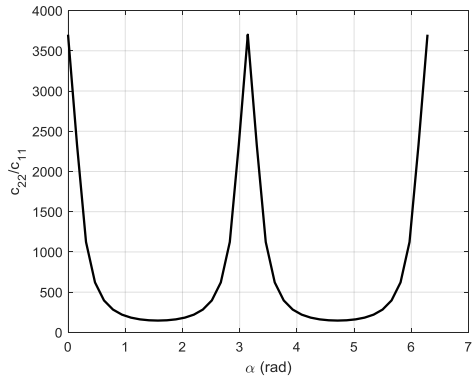

(a)

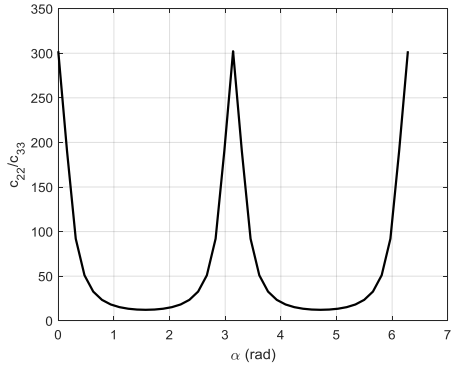

(b)

Figure 3. Case I compliance results for the parallelogram mechanism affected by position angle

(3) Case III: $\beta \neq \alpha$

Under case III where $\beta \neq \alpha$, the influence of α on the compliance ratio is investigated considering a specific value of β as shown in Figs. 5(a) and (b). It is clear that the compliance ratio at $\beta=0$ is the best, but has the largest regular fluctuation over α. The parasitic motion entry is shown in Fig. 5(c). It can be observed that at $\beta=\pi/4$ c_{23} is not less than zero, with a periodic change. c_{23} at $\beta=\pi/2$ is nearly same as that at $\beta=0$, throughout the range of α.

One can prove mathematically that under the same α, $\beta=\beta_0$ and $\beta=\beta_0+\pi$ (any value of β_0) will obtain the same compliance matrix of the parallelogram mechanism. If $\beta=\pi$ or 0, the compliance matrix, using the assigned parameters above, is expressed as below:

$$C_s = \begin{bmatrix} -\frac{1}{138000}\frac{11061\cos(\alpha)^2-11986}{3\cos(\alpha)^2+922} & 0 & 0 \\ 0 & \frac{1}{34500}\frac{7461\cos(\alpha)^2-1118386}{12\cos(\alpha)^2-1213} & -\frac{6}{575}\frac{\cos(\alpha)\sin(\alpha)}{12\cos(\alpha)^2-1213} \\ 0 & -\frac{6}{575}\frac{\cos(\alpha)\sin(\alpha)}{12\cos(\alpha)^2-1213} & \frac{1}{11500}\frac{12\cos(\alpha)^2-13}{12\cos(\alpha)^2-1213} \end{bmatrix} \quad (12b)$$

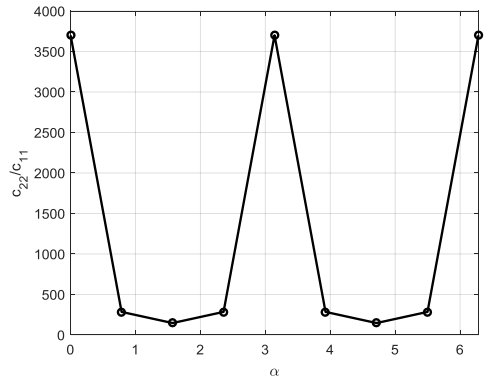

(a)

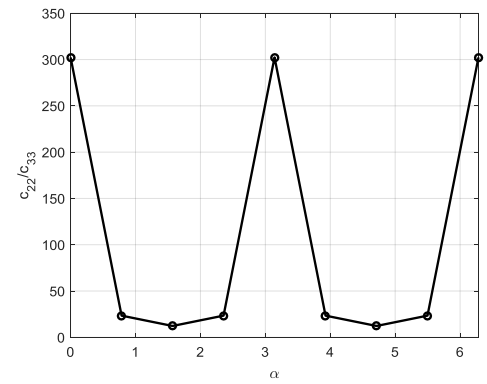

(b)

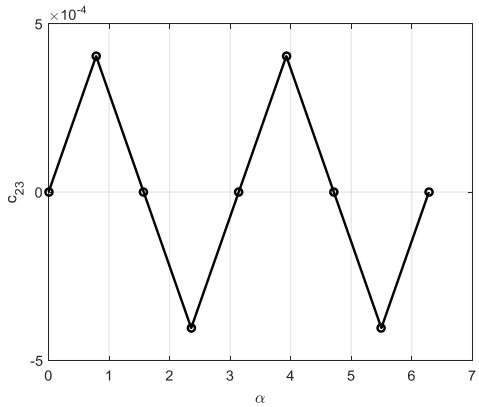

(c)

Figure 4. Case II compliance results for the parallelogram mechanism affected by position angle

It is also interesting to know that Ref. [18] also discussed the influence of the flexure hinge orientation in the parallelogram mechanism with lumped compliance, which can be explained using our position-space framework. Note that the work in [18] does not include parameter synthesis.

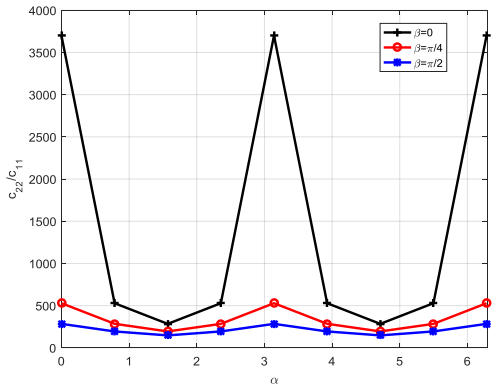

(a)

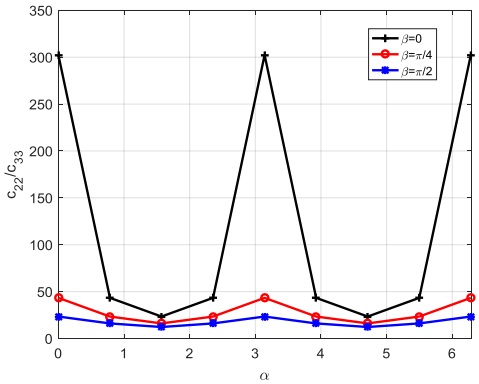

(b)

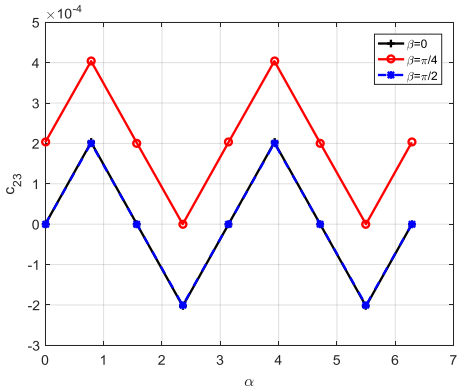

(c)

Figure 5. Case III compliance results for the parallelogram mechanism affected by position angle

IV. Compliance Modelling of an Improved Parallelogram Mechanism Using Cross-axis Joints

This section presents an improved parallelogram mechanism using cross-axis joints instead of the short-beam hinges, which is shown in Fig. 6. All cross-axis joints are identical. An extra angle parameter (γ) is introduced to denote the angle of two beams in a cross-axis joint.

The compliance modelling process of the improved parallelogram mechanism is exactly same as the one shown in Fig. 1, except there is a need of modifying the following matrices for two cross-axis joints in each leg.

$$\begin{aligned} C_{11} &= \{[R_{11}C(R_{11})^{\mathrm{T}}]^{-1} + [R_{11d}C(R_{11d})^{\mathrm{T}}]^{-1}\}^{-1} \\ C_{12} &= \{[R_{12}C(R_{12})^{\mathrm{T}}]^{-1} + [R_{12d}C(R_{12d})^{\mathrm{T}}]^{-1}\}^{-1} \end{aligned} \tag{13}$$

where

$$R_{11d} = \begin{bmatrix} \cos(\alpha-\gamma) & -\sin(\alpha-\gamma) & 0 \\ \sin(\alpha-\gamma) & \cos(\alpha-\gamma) & 0 \\ 0 & 0 & 1 \end{bmatrix}, \quad R_{12d} = \begin{bmatrix} \cos(\beta-\gamma) & -\sin(\beta-\gamma) & 0 \\ \sin(\beta-\gamma) & \cos(\beta-\gamma) & 0 \\ 0 & 0 & 1 \end{bmatrix}.$$

$$\begin{aligned} C_{21} &= \{[R_{21}C(R_{21})^{\mathrm{T}}]^{-1} + [R_{21d}C(R_{21d})^{\mathrm{T}}]^{-1}\}^{-1} \\ C_{22} &= \{[R_{22}C(R_{22})^{\mathrm{T}}]^{-1} + [R_{22d}C(R_{22d})^{\mathrm{T}}]^{-1}\}^{-1} \end{aligned} \tag{14}$$

where

$$R_{21d} = \begin{bmatrix} \cos(\gamma-\alpha) & -\sin(\gamma-\alpha) & 0 \\ \sin(\gamma-\alpha) & \cos(\gamma-\alpha) & 0 \\ 0 & 0 & 1 \end{bmatrix}, \quad R_{22d} = \begin{bmatrix} \cos(\gamma-\beta) & -\sin(\gamma-\beta) & 0 \\ \sin(\gamma-\beta) & \cos(\gamma-\beta) & 0 \\ 0 & 0 & 1 \end{bmatrix}.$$

Using the results in Eqs. (13) and (14) to replace C_{11}, C_{12}, C_{21} and C_{22} in Section 3, we can derive the compliance matrix of the improved parallelogram mechanism. We will also analyze three cases as discussed below.

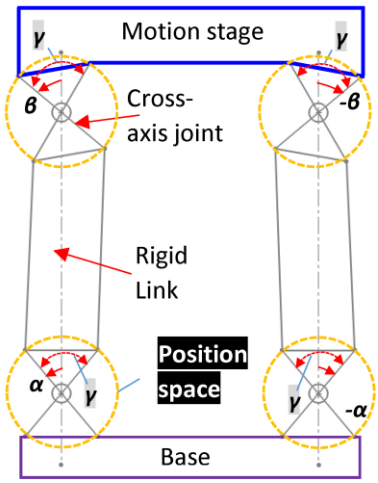

Figure 6. Schematic diagram of the improved parallelogram mechanism

(1) Case I: Any α, any β under $|\gamma|=\pi/2$

Under case I, a simple symbolic solution of the compliance matrix is obtained in Eq. (15), which is a diagonal matrix. Interestingly, the rotational parameter α or β in this compliance matrix vanishes, meaning that the compliance performance keeps unchanged in the whole position space of cross-axis joints (Fig. 7). It, however, remains unknown if other indices such as stress distribution change over α.

$$C_s = \begin{bmatrix} \frac{1}{12}\frac{T^2L^3}{EI\left(L^2+T^2\right)} & 0 & 0 \\ 0 & \frac{1}{24}\frac{L\left(3H^2L^2+3H^2T^2+2L^2T^2\right)}{EI\left(L^2+T^2\right)} & 0 \\ 0 & 0 & \frac{T^2L^3}{EI\left(2L^2T^2+3L^2W^2+3T^2W^2\right)} \end{bmatrix} \quad (15)$$

Equation (15) shows that the parameter H only affects C_{s22}, and the parameter W only influences C_{s33}.

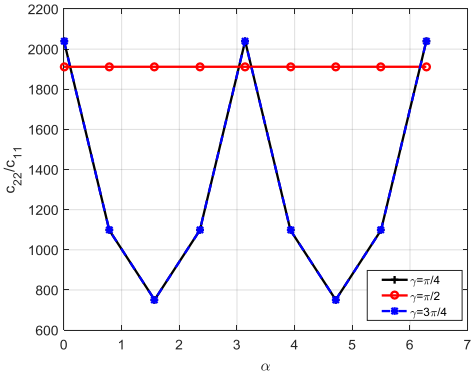

(a)

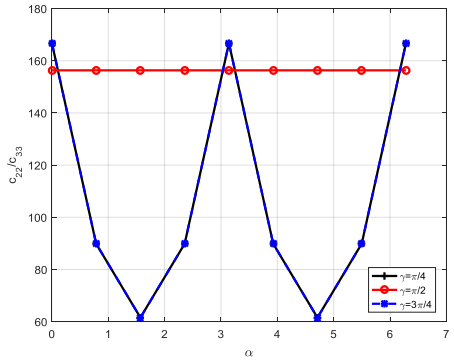

(b)

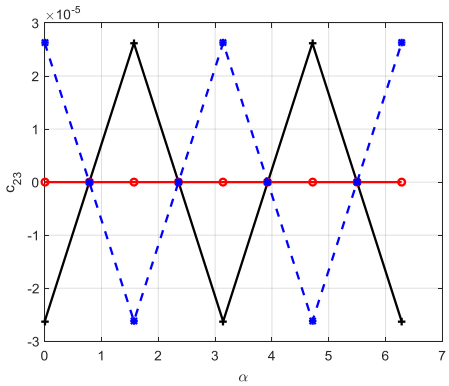

(c)

Figure 7. Comparison of Cases I and II of the improved parallelogram mechanism

(2) Case II: $\beta=-\alpha$ and $|\gamma|\neq\pi/2$

Under case II, there is no simple symbolic solution to be shown. Cases I and II are compared in Fig. 7. c_{22}/c_{11} (or c_{22}/c_{33}) at $\gamma=\pi/4$ is same as that at $\gamma=3\pi/4$, throughout the range of α. However, c_{23} at $\gamma=\pi/4$ is opposite to that at $\gamma=3\pi/4$, with a magnitude in the order of 10^{-5} rad. When $\alpha=0$ or π, the compliance ratio is the optimal, where c_{22}/c_{11} is larger than 2000 and c_{22}/c_{33} is larger than 160. When $\alpha=\pi/2$ or $3\pi/2$, the compliance ratio is the worst, with c_{22}/c_{11} larger than 700 and with c_{22}/c_{33} larger than 60.

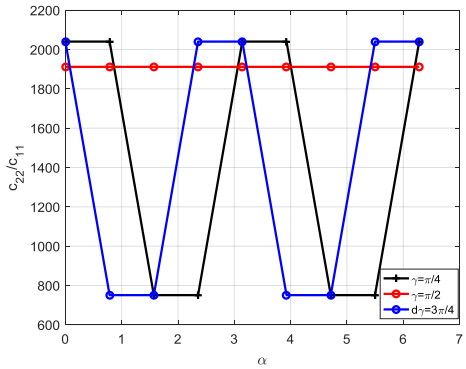

(a)

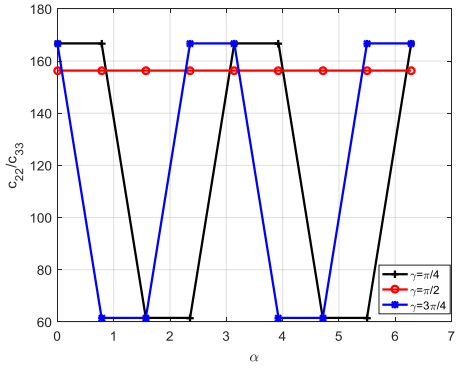

(b)

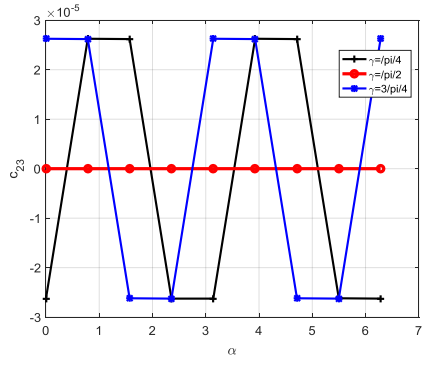

(c)

Figure 8. Comparison of Cases I and III of the improved parallelogram mechanism

(3) Case III: $\beta=\alpha$ and $|\gamma|\neq\pi/2$

Under case III, a symbolic solution of the compliance matrix can not be shown as well. Case I and Case III are compared in Fig. 8. It is shown in case III that either the compliance ratio and the parasitic motion entry change periodically, the result at $\gamma=\pi/4$ has a $\pi/4$ phase delay compared to that at $\gamma=3\pi/4$.

V. Conclusion

Utilizing the position space concept, this paper carries out a comprehensive compliance synthesis of a class of planar compliant parallelogram mechanisms, including the generic mechanism composed of short-beam hinges and the improved one composed of cross-axis joints. Analytical models have been derived to identify the influence of rotational positions on the compliance characteristics of the mechanism.

This paper presented the modelling results based on the linear modelling method, thus only the instantaneous kinetostatic characteristics have been captured, and those nonlinear characteristics such as the parasitic translation (along the X-axis) accompanying the primary motion (along the Y-axis) were not covered. Note that although the position space was defined for each of the short-beam joints in the parallelogram mechanism, the modelling results in this paper are still valid for the parallelogram mechanisms with distributed compliance.

Considering the linear compliance characteristics as the task in this paper, we can conclude the following: a) the first parallelogram (Fig. 2) has the best performance if $|\alpha|=0$ or π and $|\beta|=0$ or π; b) the second parallelogram (Fig. 6) has an unchanged performance under $|\gamma|=\pi/2$ despite the change α and β, and the second parallelogram has the best performance if $|\alpha|=|\beta|=0$ or π and $|\gamma| \neq \pi/2$. Figure 2(a) shows the parallelogram mechanism with normal arrangements of beams (i.e., $\alpha=\beta=0$). Figure 9(a) shows the parallelogram mechanism with inverted arrangements of beams (i.e., $\alpha=\beta=\pi$). Figure 9(b) shows the parallelogram mechanism with inverted arrangements of half number of beams and normal arrangements of half number of beams (i.e., $\alpha=\pi$ and $\beta=0$). Figure 10 shows several typical configurations of the improved parallelogram mechanism under $\gamma=\pi/2$. It is interesting to learn that in Fig. 9(a) all compliant beams undergo tensile forces when the motion stage is imposed a compression force, and that in Fig. 9(b) two beams suffer from compression forces and two beams suffer from tensile forces no matter whether the motion stage is compressed or not. Several compound designs composed of non-identical legs in parallel are shown in Figs. 9(c), 9(d) and 9(e) where beams in each leg either are normally arranged (Fig. 2(a)) or inversely arranged (Fig. 9(a)). These compound designs can alleviate buckling effect for any directional axial force exerted on the motion stage. We should point out that the designs in Figs. 9(b) and 9(e) may produce a load-independent primary stiffness in the lateral direction, which is independent of the axial force on the motion stage. Because there are always half number of beams undergoing compression forces (reducing the primary stiffness) and half number of beams undergoing tensile forces (increasing the primary stiffness), the overall change of primary stiffness is zero.

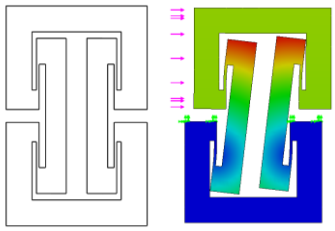

(a) Design with $\alpha=\beta=\pi$

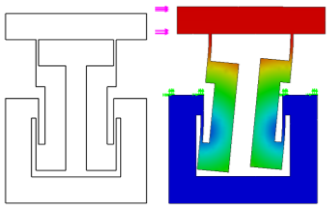

(b) Design with $\alpha=\pi$ and $\beta=0$

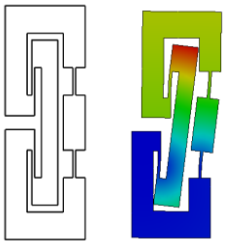

(c) A compound design I with two different legs

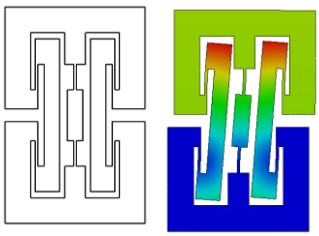

(d) A compound design II with three legs

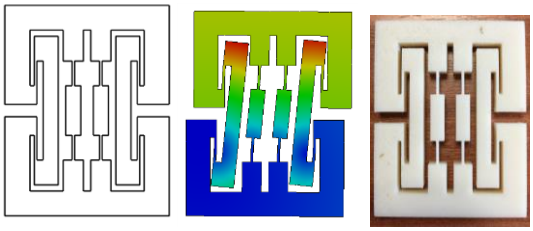

(e) A compound design II with two pairs of legs

Figure 9. Different parallelogram mechanisms

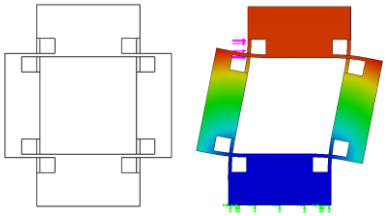

(a) Design with $\gamma=\pi/2$, $\alpha=\pi/2$, $\beta=0$

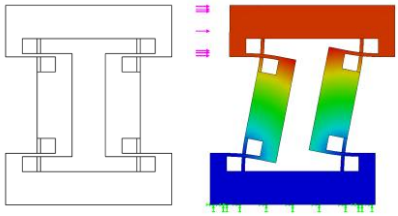

(b) Design with $\gamma=\pi/2$, $\alpha=0$, $\beta=\pi/2$

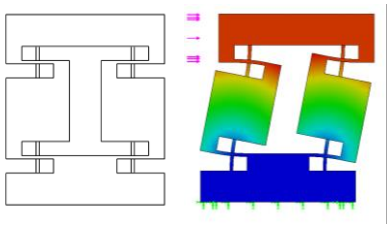

(c) Design with $\gamma=\pi/2$, $\alpha=\pi/2$, $\beta=\pi/2$

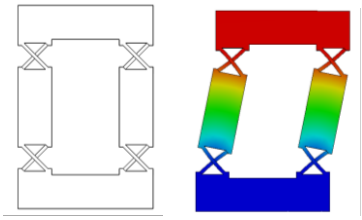

(d) Design with $\gamma=\pi/2$, $\alpha=\pi/4$, $\beta=\pi/4$

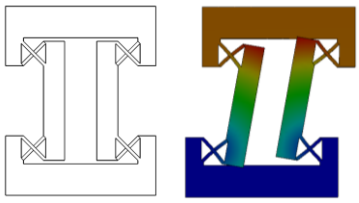

(e) Design with $\gamma=\pi/2$, $\alpha=7\pi/4$, $\beta=3\pi/4$

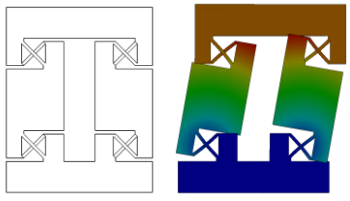

(f) Design with $\gamma=\pi/2$, $\alpha=3\pi/4$, $\beta=3\pi/4$

Figure 10. Several improved parallelogram mechanisms under $|\gamma|=\pi/2$

For more extensive applications, the position space should be combined with the stress distribution/motion range to determine the optimal design, in addition to considering the stiffness/compliance performance. Moreover, the position space method can be used to interpret the emerging good designs. For example, a parallelogram mechanism composed of four identical trapezoidal joints (with remote rotation centers), as shown in Fig. 11, can be reconfigured to the design reported in [19] with the elimination of coupled parasitic translation. This is done by rotating each joint half circle (similar to Fig. 9(a)) followed by nonlinear parametric modelling and analysis.

The future work is to synthesize other diverse types of compliant mechanisms such as the revolute joint (Fig. 12) using the similar idea presented in this paper, with a particular focus on nonlinear stiffness and motion characteristics.

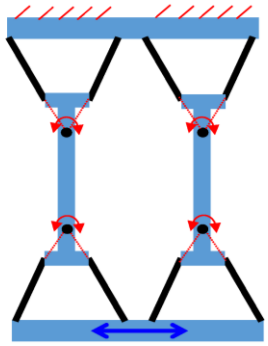

Figure 11. A parallelogram mechanism with trapezoidal joints

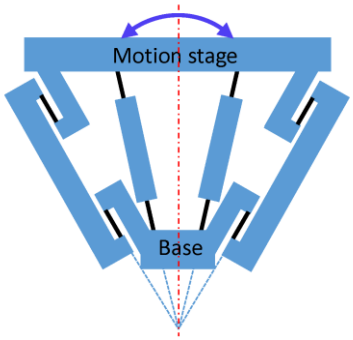

Figure 12. A revolute joint with two pairs of trapezoidal joints in parallel: one pair being normally arranged and another pair being inversely arranged

APPENDIX

$$C_s = \begin{bmatrix} \begin{bmatrix} -\frac{1}{12}\frac{L\left(3H^2L^2\cos(\alpha)^2 - 3H^2\cos(\alpha)^2T^2 - 3H^2L^2 - L^2T^2\right)}{EI\left(\cos(\alpha)^2L^2 - \cos(\alpha)^2T^2 + 3H^2 + T^2\right)}, 0, 0 \end{bmatrix}, \\ \begin{bmatrix} 0, \frac{1}{12}\frac{L\left(3H^2L^2\cos(\alpha)^2 - 3H^2\cos(\alpha)^2T^2 - 3L^2\cos(\alpha)^2W^2 + 3T^2W^2\cos(\alpha)^2 - 3H^2L^2 - 9H^2W^2 - L^2T^2 - 3T^2W^2\right)}{EI\left(\cos(\alpha)^2L^2 - \cos(\alpha)^2T^2 - L^2 - 3W^2\right)}, -\frac{1}{2}\frac{LW\left(L^2 - T^2\right)\cos(\alpha)\sin(\alpha)}{EI\left(\cos(\alpha)^2L^2 - \cos(\alpha)^2T^2 - L^2 - 3W^2\right)} \end{bmatrix}, \\ \begin{bmatrix} 0, -\frac{1}{2}\frac{LW\left(L^2 - T^2\right)\cos(\alpha)\sin(\alpha)}{EI\left(\cos(\alpha)^2L^2 - \cos(\alpha)^2T^2 - L^2 - 3W^2\right)}, \frac{L\left(\cos(\alpha)^2L^2 - \cos(\alpha)^2T^2 - L^2\right)}{EI\left(\cos(\alpha)^2L^2 - \cos(\alpha)^2T^2 - L^2 - 3W^2\right)} \end{bmatrix} \end{bmatrix} \tag{A.1}$$

REFERENCES

[1] R. V. Jones, "Some uses of elasticity in instrument design," Journal of Scientific instruments, vol. 39, no. 5, pp. 193, 1962.

[2] S. T. Smith, Flexures: elements of elastic mechanisms, New York: Gordon and Breach Science Publishers, 2000.

[3] L. L. Howell, Compliant mechanisms, New York: John Wiley & Sons, 2001.

[4] N. Lobontiu, Compliant mechanisms: design of flexure hinges: CRC press, 2002.

[5] L. L. Howell, Handbook of compliant mechanisms, New York: John Wiley & Sons, 2013.

[6] G. B. Hao, 2015, "Mobility and Structure Re-configurability of Compliant Mechanisms", Mechan. Machine Science, Vol. 36, Xilun Ding et al. (Eds):Advances in Reconfigurable Mechanisms and Robots II, 978-3-319-23326-0, 334477_1_En, Berlin: Springer (chapter 5)

[7] G. B. Hao, H.Y. Li, R. Kavanagh, 2016, "Design of Decoupled, Compact, and Monolithic Spatial Translational Compliant Parallel Manipulators Based on the Position Space", Proceedings of the IMechE, Part C: Journal of Mechanical Engineering Science, 230(3):367-378

[8] H.Y. Li, G. B. Hao, 2015, "A Constraint and Position Identification Approach for the Synthesis of Decoupled Spatial Translational Compliant Parallel Manipulators", Mechanism and Machine Theory, 90:59-83

[9] H.Y. Li, G. B. Hao, R. Kavanagh, 2016, "Position-Space-Based Compliant Mechanism Reconfiguration Approach and Its Application in Reduction of Parasitic Motion", Journal of Mechanical Design (ASME Transactions), 138(9):092301

[10] H.Y. Li, 2016. Approaches to the synthesis, modelling and optimization of spatial translational compliant parallel mechanisms. PhD Thesis, University College Cork.

[11] S. Fan, H. Liu, D. Fan, 2018. Design and development of a novel monolithic compliant XY stage with centimeter travel range and high payload capacity", Mech. Sci., 9, 161-176

[12] H. Liu, S. Fan, X. Xie, et al., 2017. "Design and modeling of a novel monolithic parallel XY stage with centimeters travel range". Advances in Mechanical Engineering, 9(11), p.168781401772962

[13] G. B. Hao, 2017, "Determinate design and analytical analysis of a class of symmetrical flexure guiding mechanisms for linear actuators", Journal of Mechanical Design (ASME Transactions), 139(1):012301

[14] G. B. Hao, 2017, "Determinate synthesis of symmetrical, monolithic tip-tilt-piston flexure stages", Journal of Mechanical Design (ASME Transactions), 139(4), 042303

[15] G. B. Hao, F. Dai, X. He, Y. Liu, 2017, "Design and analytical analysis of a large-range tri-symmetrical 2R1T compliant mechanism", Microsystem Technologies, 23:4359-4366

[16] G. B. Hao, X. W. Kong, 2012, "A Novel Large-Range XY Compliant Parallel Manipulator with Enhanced out-of-Plane Stiffness", Journal of Mechanical Design (ASME Transactions), 134 (6):061009

[17] G. B. Hao, X. W. Kong, 2013, "A Normalization-Based Approach to the Mobility Analysis of Spatial Compliant Multi-Beam Modules", Mechanism and Machine Theory, 59 (1): 1-19.

[18] P. Graser, S. Linß, L. Zentner, R. Theska, "On the influence of the flexure hinge orientation in planar compliant mechanisms for ultra-precision applications, " in: Proc. of the 59th International Scientific Colloquium, 59th Ilmenau Scientific Colloquium, Ilmenau, Germany, 2017, pp. 1–10.

[19] H. Z. Zhao, S. S. Bi, J. J. Yu, 2012. "Design of a family of ultra-precision linear motion mechanisms." Journal of Mechanisms and Robotics, 4(4), p.041012.